Title
Near-IR and CP-OCT imaging of suspected occlusal caries lesions

Journal
Lasers in Surgery and Medicine, 49(3)

ISSN
0196-8092

Authors
Simon, Jacob C
Kang, Hobin
Staninec, Michal
et al.

Publication Date
2017-03-01

DOI
10.1002/lsm.22641

Peer reviewed

HHS Public Access

Author manuscript

Lasers Surg Med. Author manuscript; available in PMC 2018 March 24.

Published in final edited form as:

Lasers Surg Med. 2017 March ; 49(3): 215–224. doi:10.1002/lsm.22641.

Near-IR and CP-OCT Imaging of Suspected Occlusal Caries Lesions

Jacob C. Simon, **Hobin Kang**, **Michal Staninec**, **Andrew T. Jang**, **Kenneth H. Chan**, **Cynthia L. Darling**, **Robert C. Lee**, and **Daniel Fried**

University of California, San Francisco, San Francisco, CA 94143-0758

Abstract

Introduction—Radiographic methods have poor sensitivity for occlusal lesions and by the time the lesions are radiolucent they have typically progressed deep into the dentin. New more sensitive imaging methods are needed to detect occlusal lesions. In this study, cross-polarization optical coherence tomography (CP-OCT) and near-IR imaging were used to image questionable occlusal lesions (QOC's) that were not visible on radiographs but had been scheduled for restoration on 30 test subjects.

Methods—Near-IR reflectance and transillumination probes incorporating a high definition InGaAs camera and near-IR broadband light sources were used to acquire images of the lesions before restoration. The reflectance probe utilized cross-polarization and operated at wavelengths from 1500–1700-nm where there is an increase in water absorption for higher contrast. The transillumination probe was operated at 1300-nm where the transparency of enamel is highest. Tomographic images (6×6×7 mm^3) of the lesions were acquired using a high-speed swept-source CP-OCT system operating at 1300-nm before and after removal of the suspected lesion.

Results—Near-IR reflectance imaging at 1500–1700-nm yielded significantly higher contrast ($p<0.05$) of the demineralization in the occlusal grooves compared with visible reflectance imaging. Stains in the occlusal grooves greatly reduced the lesion contrast in the visible range yielding negative values. Only half of the 26 lesions analyzed showed the characteristic surface demineralization and increased reflectivity below the dentinal-enamel junction (DEJ) in 3D OCT images indicative of penetration of the lesion into the dentin.

Conclusion—This study demonstrates that near-IR imaging methods have great potential for improving the early diagnosis of occlusal lesions.

1. INTRODUCTION

Occlusal caries lesions are routinely detected in the United States using visual/tactile (explorer) methods coupled with radiography. Radiographic methods have poor sensitivity for detecting occlusal lesions, and by the time the lesions are radiolucent they have typically progressed deep into the dentin at which point it is too late for non-surgical intervention to

Corresponding Author: Daniel Fried, Department of Preventive and Restorative Dental Sciences, University of California, San Francisco, San Francisco, 707 Parnassus Ave. 94143, Phone: (415) 502-6641, Fax: (415) 502-6642, daniel.fried@ucsf.edu.

None of the authors have potential Conflicts of Interest that need to be disclosed.

be effective [1]. Some of these “hidden” lesions may show up in radiographs but most do not [2,3]. Such hidden lesions are more common today with the widespread use of fluoride and new more sensitive methods are needed to detect these lesions. Fluorescence based methods that detect the fluorescence of porphyrin molecules found in bacteria have been developed for detecting hidden lesions, however they suffer from a high rate of false positives and neither the depth or exact position of the lesions is indicated [4,5]. Recent studies utilizing the Practice Based Research Network (http://www.nationaldentalpbrn.org) [6–8] funded by the National Institutes of Health, indicated that 1/3 of all patients have a questionable occlusal caries lesion (QOC). QOC's can be defined as an occlusal surface without cavitation or radiographic radiolucencies, but caries is suspected due to shadows, roughness, surface opacities or staining. After monitoring QOC's for 20 months in the PBRN study, 90% did not require surgical intervention or restoration. Furthermore, the identification of occlusal lesions penetrating to the dentin is poor with an accuracy of ~50% [9,10].

Enamel manifests its highest transparency near 1300-nm where the scattering coefficient of enamel is 20–30 times lower than it is at visible wavelengths [11,12]. Due to the high transparency of enamel, novel imaging configurations are feasible in which the tooth can be imaged from the occlusal surface after shining light at and below the gum line, which we call occlusal transillumination [13–17]. Upon demineralization the scattering coefficient of enamel increases by 1–2 orders of magnitude at 1300-nm to yield high contrast between sound and demineralized enamel for caries detection [18]. Therefore, this wavelength range is ideally suited for the transillumination of occlusal caries lesions. Carious lesions appear dark in transillumination images due to the combination of increased scattering and absorption by the lesion that reduces optical transmission. Recently, a commercial near-IR transillumination system has been introduced called the Diagnocam from Kavo (Biberach, Germany) that uses an occlusal transillumination probe with 780-nm light [19,20]. We previously investigated using transillumination imaging at 830-nm which has the advantage of utilizing a low-cost silicon CCD sensor optimized for the near-IR. The 830-nm system was capable of higher performance than visible systems, but the contrast was significantly lower than 1310-nm and simulated lesions could not be imaged through the full enamel thickness [21]. Other groups have confirmed the high potential of the near-IR for imaging dental decay [22,23].

There are other important advantages of imaging dental decay in the near-IR. Stains that are common on tooth occlusal surfaces do not interfere at near-IR wavelengths since none of the known chromophores absorb light in the near-IR beyond 1300-nm [13,23]. More recently, Almaz et al. demonstrated that it was necessary to use near-IR wavelengths greater than 1150-nm to avoid significant interference from stains when measuring lesion contrast in reflectance and transillumination modalities [24]. Therefore stains can be easily differentiated from actual demineralization in the near-IR range, which is not possible at visible wavelengths. Chung et al. [25] indicated that the absorption due to stains contributed more to the lesion contrast than actual demineralization at visible wavelengths [26]. Since it is impractical to remove stains from the deep grooves and fissures on tooth occlusal surfaces, lack of interference from stains at longer near-IR wavelengths is a significant advantage.

Additionally, reflectance imaging at wavelengths greater than 1300-nm have yielded extremely high contrast of early demineralization [23,25,27–30]. More recent near-IR imaging studies suggest that longer near-IR wavelengths coincident with high water absorption namely, 1450-nm or 1500–1700-nm, yield the highest contrast of demineralization on tooth surfaces [29,30]. We hypothesize that higher water absorption at these wavelengths reduces the reflectivity in the sound enamel and the underlying dentin resulting in even higher contrast between sound and demineralized enamel than that observed at 1300-nm. Hyperspectral reflectance measurements by Zakian et al. [23] show that the sound regions of the tooth appear darker at wavelengths coincident with higher absorption by water.

Near-IR imaging reflectance and transillumination imaging methods are ideally suited for caries screening, i.e., detecting that lesions are present on tooth surfaces. Optical coherence tomography (OCT) is a noninvasive technique for creating cross-sectional images of internal biological structure [31]. Several groups have used OCT and PS-OCT to image dental caries on both smooth surfaces and occlusal surfaces [32–35]. OCT is poorly suited for rapid caries screening since it takes too long to acquire images of all tooth surfaces, however it is extremely valuable for acquiring 3D images of suspect lesions to assess the depth of lesion penetration to aid in diagnosis. We have demonstrated that polarization sensitivity is necessary for accurate depth-resolved measurements of the severity of demineralization both *in vitro* and *in vivo* [35–37]. Quantitative depth resolved measurements are useful for clinical studies and for monitoring the state of early lesions and our studies indicate that polarization sensitivity provides considerable advantages for the measurement of early demineralization on tooth surfaces [35–37]. We postulate that OCT is ideally suited for monitoring and improving the diagnosis of QOC's. Even though the optical penetration of near-IR light can easily exceed 7-mm through sound enamel to image lesions on proximal surfaces with high contrast [21], the large increase in light scattering due to demineralization [18] typically limits optical penetration in highly scattering lesions (also dentin and bone) to 1–2 mm, thus cutting off the OCT signal before it reaches the dentinal-enamel junction (DEJ). However, most occlusal lesions rapidly spread laterally under the enamel upon contacting the more soluble softer dentin, with the largest lateral spread usually at the DEJ and that lateral spread can be detected under the sound enamel with OCT.

We have carried out three prior clinical studies involving near-IR transillumination imaging [16,38,39] and one recent study involving near-IR reflectance [39]. In our most recent near-IR imaging clinical study [39], we employed three near-IR imaging probes to screen for lesions on premolars scheduled for extraction, and we demonstrated that near-IR image methods can achieve higher diagnostic performance than radiographs for the detection of lesions on both proximal and occlusal surfaces. In 2011, we carried out a clinical study of teeth with non-cavitated occlusal caries lesions that were not visible on radiographs. Teeth with suspect lesions were examined using near-IR occlusal transillumination at 1300-nm and polarization optical coherence tomography prior to restoration [38]. In that study, we used a relatively slow time-domain OCT system (150-Hz scan rate) to acquire individual b-scan images across the occlusal lesions. That study demonstrated that near-IR transillumination at 1300-nm can be used to image occlusal caries lesions with high contrast *in vivo* and that OCT can be used to detect lesion penetration into dentin. That study also indicated that it is

necessary to acquire entire tomographic OCT scans to resolve the lateral spread of the lesions in all directions as opposed to single b-scans. This requires a high-speed OCT system and in this study we employ a swept-source CP-OCT system operating at a scan rate of 33-kHz to acquire entire 3D images of the lesions.

We also use near-IR occlusal transillumination and reflectance probes to acquire high-resolution images of suspected occlusal lesions using a high-definition (1024 × 1280 element) InGaAs camera and measured the lesion contrast with both imaging modes. In addition, to avoiding the interference of stains at wavelengths beyond 1200-nm, which is likely the principal reason for the misdiagnosis of QOC's, we postulate that the acquisition of both near-IR reflectance and transillumination images will help avoid false positives due to specular reflection or anatomical features. Moreover, since superficial (shallow) demineralization in the pits and fissures of the occlusal surfaces may not be visible in transillumination images while being visible with high contrast in reflectance images, the differential appearance will be useful for assessing lesion severity. Namely, demineralization that is visible only in near-IR reflectance images is likely localized to the outer enamel and surgical intervention is not needed.

2. MATERIALS & METHODS

2. Experimental methods

2.1. Patient recruitment—After obtaining IRB approval and written informed consent, 30 participants were recruited from the predoctoral clinics of the University of California, San Francisco, School of Dentistry. Adult subjects aged 18 to 60 with a questionable occlusal lesion (QOC) that was not apparent on a radiograph and had been scheduled for restoration were recruited. A total of 30 teeth were imaged in the study. Four samples were excluded after imaging with one due to frank cavitation, two due to preexisting sealants on the occlusal surface, and the images were unreadable for one lesion.

2.2. Visible images—A Dino-Lite digital USB microscope, Model AM7013MZT, AnMO Electronics Corp. (New Taipei City, Taiwan) equipped with a dental mirror was used to acquire visual digital images, both wet and dry, of the patients’ teeth prior to near-IR imaging. The digital microscope captures 5 mega-pixel (2592 ×1944) color still images and video. Eight white LED lights contained in the camera illuminate the teeth and the device features polarization optics to eliminate specular reflection and reduce glare. Visual images were taken for reference and comparison with near-IR techniques at the beginning of each imaging session.

2.3. Near-IR imaging probes with InGaAs FPA—Two near-IR imaging probes were utilized to capture cross-polarized reflectance and occlusal transillumination videos of samples prior to restoration. The cross-polarized reflectance probe used a broadband light from a tungsten-halogen lamp, Model HL-2000 (Ocean Optics, Dunedin, FL) filtered using a long pass 1500-nm filter, Model FEL1500 (ThorLabs, Newton, NJ) and delivered to the probe through a glass fiber optic waveguide (Dolan-Jenner, Boxborough, MA) to yield light detectable in the range from 1500–1700-nm. The light emitted from the waveguide is incident on a polarizing beam splitter cube, Model PBS054 (Thorlabs) where a single linear

polarization state is reflected down through the hollow width of the probe and onto the sample surface. The light interacts with the tooth and is reflected or scattered back to a right-angled mirror and directed down the imaging tube to the focal plane array. A second adjustable linear polarizer, Model MPIRE-100-C (Thorlabs) was inserted into a rotating element and oriented orthogonally to the polarization state of the first to eliminate specular reflected light from reaching the detector. The reflectance probe delivered a 6–10-mW cone of light over a circular area 1.5-cm in diameter.

The near-IR occlusal transillumination probe employed light centered at 1310-nm generated using a superluminecent diode with a 50-nm bandwidth. Fiber optic cables were used to deliver the light into two diffusing elements made of Teflon. The diffusing elements are positioned using copper tubes that direct the light below the cementum-enamel junction (CEJ) into the gingival tissue from both the lingual and facial sides at a shallow angle. Light that enters the tooth diffuses throughout its interior and out the occlusal tooth surface. A right-angled mirror reflects the emitted light down the imaging tube through the relay optics and onto the focal plane array of the camera. The probe is designed to rotate 180-degrees for the imaging of both upper and lower teeth. The occlusal transillumination probe delivered a 6–10-mW cone of light onto the lingual and buccal surfaces with a circular area 3-mm in diameter.

Each individual probe is attached to common optical components consisting of two iris diaphragms, f=60-mm AC254-060-C and f=150-mm AC254-150-C (Thorlabs) near-IR achromatic lenses, coupled to a high sensitivity InGaAs focal plane array (FPA), Model GA1280J (Sensors Unlimited, Princeton, NJ) with a 1280 × 1024 pixel format and 15-μm pixel pitch. A 360-degree rotation element allows simple rearrangement of the imaging probe to access both the maxillary (upper) and mandibular (lower) teeth. The assembly is physically supported via an aluminum post attached to an elastic band wrapped around the forearm of the clinician. A power supply and output cable attaches to the backside of the camera and connects the instrumentation with computers and programming through a mesh bundle. Diagrams of each probe can be found in reference [39]. Probes were sterilized in an autoclave before each imaging session.

2.4. Visible and near-IR clinical imaging protocol—Each tooth was imaged *in vivo* with the visible and near-IR imaging systems (OCT and near-IR probes) while viewing a live video feed of the captured images on a computer monitor before the tooth was restored. After the preparation was cut into the occlusal surface, visible and OCT images were acquired of the sample. Imaging was employed in the following order: (1) Conventional photos of the teeth were taken (both wet and air dried) using a digital camera. (2) Cross-polarized near-IR reflectance images were acquired for the detection of surface demineralization in the pits and fissures and other external (surface) signs of decay. (3) Two OCT scans were performed on the occlusal surface of each tooth before and after the tooth was prepared for a restoration. During near-IR reflectance and OCT imaging an air spray was employed to dry the tooth surface and increase lesion contrast. The air spray was also used to remove air bubbles during near-IR transillumination imaging and to prevent moisture build up on the OCT sensor window. Imaging was carried out in a separate clinical research room outside the predoctoral clinics from where the test subjects were recruited and the

clinicians carrying out the initial diagnosis, treatment plan and cavity preparations had no access to the imaging data.

2.5 Image Analysis—Visible images were analyzed using the image analysis package, IgorPro (Wavemetrics, Lake Oswego, OR). Both the suspected lesion area and sound tissue intensities were measured using a freehand Region of Interest (ROI) tool in order to calculate the mean intensities from each region. Visible-light reflectance lesion contrast was calculated using the equation $(I_L - I_S)/I_L$, where I_L is the intensity of the lesion area and I_S is the intensity of the surrounding sound area. Increased scattering from demineralized tissue produces a greater intensity signal and I_L should be higher than I_S. The reported contrast values can range from 0 to 1 where a 0 value represents no contrast, a 1 value represents maximum contrast, and negative values represents inverse contrast. The reported lesion contrast ranges from 0 to 1 when the lesion intensity is greater than the measured sound intensity. A negative contrast can occur when the measured sound intensity exceeds the lesion intensity and the reported values do not have a confined range. Contrast values were compared with near-IR measurements using repeated measures one-way analysis of variance (ANOVA) followed by Tukey-Kramer post-hoc multiple comparison tests using InStat statistical software (GraphPad, San Diego, CA).

Near-IR cross-polarized reflectance and occlusal transillumination videos were analyzed using software developed using LabView (National Instruments, Austin, TX). Near-IR videos were screened frame by frame and the single best lesion image was selected for analysis. A circular ROI was used to capture the whole occlusal tooth surface (excluding edges) and the mean of this ROI was used as the threshold for sound tissue. Sample images were then converted into contrast maps by replacing each pixel value with a new contrast value calculated using the equation $(I_L - I_S)/I_L$ for reflectance and $(I_S - I_L)/ I_S$ for transillumination due to their different lesion appearance. Using the contrast maps, areas of similar contrast from the regions identified by the clinicians were selected as the lesion areas and the mean contrast of those selected lesion areas was calculated.

2.6 Cross-Polarization (CP-OCT) System—A cross-polarization OCT system purchased from Santec (Komaki, Aichi, Japan) was used to acquire 3D tomographic images *in vivo*. This system acquires only the cross-polarization image (CP-OCT), not both the cross and co-polarization images (PS-OCT). The device, Model IVS-300-CP, utilizes a swept laser source; Santec Model HSL-200-30 operating with a 33 kHz a-scan sweep rate. The interferometer is integrated into the handpiece which also contains the microelectromechancial (MEMS) scanning mirror and the imaging optics. This CP-OCT system is capable of acquiring complete tomographic images of a volume 6 × 6 × 7-mm in size in ~ 3 seconds. The body of the handpiece is 7 × 18-cm with an imaging tip that is 4-cm long and 1.5-cm across. This system operates at a wavelength of 1,321-nm with a bandwidth of 111-nm with a measured axial resolution in air of 11.4-μm (3-dB). The lateral resolution is 80-μm ($1/e^2$) with a transverse imaging window of 6 × 6-mm and a measured imaging depth of 7-mm in air. The polarization extinction ratio was measured to be 32-dB.

We previously developed a small sleeve made out of Delrin that fits over the window and prevents tooth structure from coming in direct contact with the window of the scanner.

Cellophane film is used as an infection control barrier on the handpiece which we found only minimally interferes with the images. The sleeve was placed in direct contact with the tooth surface and it prevents damage to the window covering the OCT scanner. The Delrin sleeve was sterilized by autoclave prior to each procedure.

During clinical procedures the images were acquired by positioning the scanner against the tooth occlusal surface while acquiring real-time *en face* images of the tooth surface.

2.7. Analysis of CP-OCT images—CP-OCT scans were analyzed using software that we developed using LabView (National Instruments, Austin, TX). Tomographic images of the sample were reconstructed from the cross-polarization image. Background subtraction was carried out by subtracting the mean reflectivity of 5000 data points measured in air from the top 100 pixels (~0.8-mm) of the 50 unprocessed a-scans (~1.0-mm) outside the sample area. The images were convolved with a Gaussian filter (3×3 filter, sigma=4) to reduce speckle noise. The 5×5 rotating kernel transformation (RKT) technique was applied in x–z and y–z spaces to emphasize thin edges while further suppressing speckle noise. Selected a-scans were chosen from acquired b-scans which contained subsurface reflections 2 to 3-mm below the surface adjacent to the fissures with occlusal lesions characteristic of increased reflectivity at the DEJ. The reflectance at the lesion surface in the center of the fissure was very strong and the OCT signal is quickly attenuated. However, lesions that penetrate to the DEJ typically spread laterally in the less acid resistant dentin so adjacent areas of the lesion are located under sound enamel and show up in OCT images as strong reflections well below the tooth surface, usually at the position of the DEJ. These b-scans typically have two areas of increased reflectivity corresponding to the tooth surface or lesion surface (top arrow in Fig.1B) and the position of the DEJ or the subsurface lesion (lower arrow in Fig. 1B). The lesion depth or distance separating the peaks at the tooth surface and lesion position of the dentin or DEJ was measured. For tooth samples prepared for restoration, the depth or distance separating the peaks at the tooth surface and internal floor of the preparation was measured. Aviso 3D software (FEI, Hillsboro, OR) was used to manipulate the 3D CP-OCT images to generate 3D volumetric renderings and movies.

3. RESULTS

Figure 1 shows a lesion for which CP-OCT clearly showed that the lesion in the fissure had penetrated beyond the DEJ and spread laterally under the adjacent enamel. In the visible light reflectance image, Fig. 1A, only the dark stain in the fissure is visible. A CP-OCT b-scan image is shown in Fig. 1B. Increased light scattering due to demineralization is shown in white. The thin dotted white line shows the position of the tooth surface and the red dotted line shows the position of the dentinal enamel junction (DEJ). The top red arrow indicates a strong reflective signal near the tooth surface in the fissure and the scattering is strong enough to cause complete loss of signal beneath the lesion. This combination of signals is the telltale signature that a lesion is present. There is a corresponding strong signal to the right of the fissure at the position of the DEJ (upward pointing arrow). This indicates the lesion has spread to the right of the lesion beneath the DEJ. Figure 1C is a 3D volumetric rendering of the entire 6 × 6-mm CP-OCT image and areas of high subsurface reflectivity are indicated in white. From the volumetric rendering of Fig. 1C it can be seen that the

lesion has penetrated to the DEJ, at the position of the red arrows, and there are large areas of lateral spread into dentin at both ends of the fissure. This is more clearly evident in the attached 3D movie (Movie1.mpg). The near-IR reflectance image shows areas of demineralization and the stains are not visible. Areas of demineralization appear whiter and with high contrast. A CP-OCT b-scan across the cavity preparation is shown in Fig. 1E acquired at the position of the green dotted line in the visible reflectance image of Fig. 1F showing the tooth after the preparation. The depth was ~ 2.2-mm and the preparation was fairly large extending well beyond the fissure.

In Fig. 2 another tooth with a stained fissure is shown which appears to have a lesion of similar severity to that of Fig. 1 viewed in visible light. The CP-OCT b-scan image in Fig. 2B shows a very shallow V-shaped lesion in the center of the fissure (red arrow) which causes only a slight increase in reflectivity and does not completely attenuate the signal below it. No deeper signal is apparent near the DEJ on either side of the fissure. Figure 2C shows a volumetric rendering of the CP-OCT 3D image showing the fissure area (yellow dots) and no subsurface demineralization is visible in areas peripheral to the fissure. The near-IR image in Fig. 2D shows a narrow band of demineralization confined to the center of the fissure and the contrast is weaker than in Fig. 1 suggesting that the surface demineralization is less severe. The cavity preparation is shown in Figs. 2 E & F and it is similar in depth (1.9-mm) and breadth to that of Fig. 1 (2.2-mm).

The tooth shown in Fig. 3 manifests a shadow that is clearly visible peripheral to the fissure. The shadow is demarcated by the yellow dots in Fig. 3A while the lesion is surrounded by the red dots. There was no lateral spread of the lesion in the demarcated shadow area (yellow dots) evident in the surface rendering of the CP-OCT 3D image, Fig. 3B, or in the reflectance and transillumination near-IR images, Figs. 3C & D. Since stain is not visible in the near-IR this suggests that the shadow or tooth discoloration is caused by stained or "affected" dentin and not demineralized dentin. The cavity preparation penetrates to the dentin, Fig. 3E, but the size of the preparation shown in Fig. 3F appears smaller than the area of the stain in Fig. 3A.

Figure 4 shows a tooth with a large interproximal lesion that is visible in the near-IR images, Figs. 4B and 4C, with high contrast but was not apparent at visible wavelengths, Fig. 4A. This tooth was included in the study because it was also diagnosed with occlusal decay in the central groove. Stain is present in the groove, Fig. 4A, but no demineralization is visible in the groove at near-IR wavelengths, Figs. B & C, or with CP-OCT. Figures 4E–G show 3D renderings of the CP-OCT scan along with an extracted b-scan image showing the rise in reflectivity caused by the subsurface interproximal lesion. This example also demonstrates how OCT images taken from the occlusal surface can be used for the diagnosis of lesions on tooth proximal surfaces. Thirty teeth were imaged and four were rejected, two had sealants, one had frank cavitation and the images were unreadable for a 4th tooth. A fifth tooth was diagnosed with an occlusal lesion and an interproximal lesion. Although the large interproximal lesion was clearly evident in the near-IR and OCT images there was no demineralization present in the occlusal fissure and it was also rejected from the statistical analysis. Twenty-five teeth were analyzed and the contrast between the sound and demineralized areas of the lesion were measured using cross-polarized visible light

reflectance, cross-polarized near-IR reflectance at 1500–1700-nm, and near-IR occlusal transillumination at 1300-nm. In addition, the CP-OCT images taken before and after lesion removal were analyzed to determine whether there was lateral spread of the lesion beneath the DEJ and the maximum depth of penetration of the lesion and the depth of the cavity preparation were recorded. The mean lesion contrast values and the mean lesion and preparation depths are tabulated in Table I. Out of the twenty-six teeth analyzed, CP-OCT analysis indicated that 13/26 of the lesions had penetrated to the dentin and that there was lateral spread under the enamel. Near-IR and CP-OCT images showed that demineralization was present on twelve more teeth but there was no evidence of lateral spread of these lesions in dentin and on one tooth the near-IR and CP-OCT images showed that no demineralization was present on the occlusal surface (Fig. 4).

4. DISCUSSION

In this study, we utilized CP-OCT and near-IR imaging at 1300 and 1500–1700-nm to image occlusal lesions that were not visible on radiographs but had been scheduled for restoration based on visual and tactile examination. Such lesions are commonly referred to as questionable occlusal caries (QOCs) due to the poor diagnostic performance of visual and tactile methods. Clinicians are forced to rely on these methods due to the extremely low sensitivity of radiographs for early occlusal lesions. The lesion contrast measured using near-IR reflectance at 1500–1700-nm was markedly higher than for visible light reflectance. The contrast approached 0.5 which is remarkably high. Demineralization increases light scattering and increases the amount of light reflected (backscattered) from the tooth surface at both visible and near-IR wavelengths, therefore demineralization should yield high positive contrast. If stains are not present, "white spot lesions" of high contrast are visible on tooth surfaces. The mean lesion contrast was negative in this study for visible wavelengths, indicating that the demineralization was completely masked by stain. This suggests that diagnosis is unreliable for the pits and fissures of occlusal surfaces in the visible range and that longer near-IR wavelengths are much better suited for assessing lesion presence. Demineralized surfaces are typically more porous increasing the retention of stains so more often than not stained surfaces are also demineralized. However, as demonstrated in this study, surfaces can be stained without any demineralization, particularly the pits and fissures, and that stain masks the degree of demineralization present.

3D CP-OCT images showed lateral spread for 13 out of the 26 lesions analyzed in this study. This is consistent with the findings of the PBRN [9,10]. Since none of the lesions were visible on the radiographs, at a minimum this potentially represents an improvement of sensitivity of over 50%. Unfortunately, there is no gold standard for confirming lesion penetration. The depth and size of the cavity preparation is the only data available since the teeth were not extracted. One would anticipate that the lesions for which the spread into dentin was confirmed with OCT would have significantly higher cavity preparation depths than those smaller lesions for which the spread was not evident. However, as can be seen in Table I, the depths of the preparations were not significantly different, moreover even though no demineralization was visible in either the near-IR images or the CP-OCT image for the stained fissure for the tooth shown in Fig. 4, a sizable preparation was still cut along the entire length of the occlusal groove, measuring ~ 2.4-mm. Therefore, it is clear that the

depth of the preparation is not a reliable confirmation that the lesion actually penetrated to the dentin. In fact, these results suggest that many of the clinicians based their diagnosis of the occlusal caries lesions on stain in the grooves, which is clearly unreliable. Moreover, accurate visual and tactile diagnosis is highly dependent on the training and experience of the clinician. In our prior similar study utilizing a much slower time-domain PS-OCT system that only acquired individual b-scans a higher percentage of the QOC's (~87%) manifested a spread into the dentin. In that study a clinician with more than 30 years of experience diagnosed all the lesions prior to the study while in this study the lesions were diagnosed in the predoctoral clinic with several different faculty mentors. It is also difficult to identify if sealants or restorations are present using visual and tactile examination and near-IR imaging methods were able to identify that sealants were present for 2/30 lesions.

Clinicians spend more time replacing failed composite restorations than placing new ones and they are difficult to identify when properly color matched. Composite restorations are much easier to visualize at near-IR wavelengths that are more highly by water due to large differences in water absorption [25,40] between dental hard tissues and composites. We have demonstrated that near-IR imaging is also well suited for the detection of secondary caries lesions around composite restorations and under sealants on occlusal surfaces [41,42].

This study further demonstrates the utility of CP-OCT for the diagnosis of QOC's and this is the first clinical study utilizing a fast swept-source system capable of acquiring entire 6 × 6 × 7-mm 3D images to determine the lesion spread in all directions. This was also the first clinical study to compare the image contrast of occlusal lesions in the visible and near-IR *in vivo*. The very high lesion contrast attained for near-IR reflectance at 1500–1700-nm is very promising. The acceptance of visible and fluorescence based caries imaging systems has been limited by the high number of false positives due to stains, particularly on tooth occlusal surfaces, and the ability to acquire images of lesions free of interference of stain is likely to have a greater impact on caries detection. In addition, near-IR imaging methods free of interference of stains can yield quantitative measures of lesion severity that are less subjective and less dependent on the training and experience.

Supplementary Material

Refer to Web version on PubMed Central for supplementary material.

Acknowledgments

The authors acknowledge the support of NIH Grants RO1-DE14698 and R01-DE17869.

This work was supported by NIH/NIDCR Grants R01-DE14698 and R01-DE17869.

REFERENCES

1. Fejerskov, O., Kidd, E., editors. Dental Caries: The Disease and its Clinical Management. Oxford: Blackwell; 2003.
2. Boston DW. Incipient and hidden caries. Dental clinics of North America. 2005; 49(4):xi–xii.
3. Ricketts D, Kidd E, Weerheijm K, de Soet H. Hidden caries: what is it? Does it exist? Does it matter? International dental journal. 1997; 47(5):259–265. [PubMed: 9448806]

4. Lussi A, Imwinkelried S, Pitts N, Longbottom C, Reich E. Performance and reproducibility of a laser fluorescence system for detection of occlusal caries in vitro. Caries Res. 1999; 33(4):261–266. [PubMed: 10343088]
5. Shi XQ, Welander U, Angmar-Mansson B. Occlusal caries detection with Kavo DIAGNOdent and Radiography:An in vitro comparison. Caries Res. 2000; 34:151–158. [PubMed: 10773633]
6. Makhija SK, Gilbert GH, Funkhouser E, Bader JD, Gordan VV, Rindal DB, Bauer M, Pihlstrom DJ, Qvist V. National Dental Practice-Based Research Network Collaborative G. The prevalence of questionable occlusal caries: findings from the Dental Practice-Based Research Network. J Am Dent Assoc. 2012; 143(12):1343–1350. [PubMed: 23204090]
7. Makhija SK, Gilbert GH, Funkhouser E, Bader JD, Gordan VV, Rindal DB, Pihlstrom DJ, Qvist V. National Dental PCG. Characteristics, detection methods and treatment of questionable occlusal carious lesions: findings from the national dental practice-based research network. Caries Res. 2014; 48(3):200–207. [PubMed: 24480989]
8. Makhija SK, Gilbert GH, Funkhouser E, Bader JD, Gordan VV, Rindal DB, Qvist V, Norrisgaard P. National Dental PCG. Twenty-month follow-up of occlusal caries lesions deemed questionable at baseline: findings from the National Dental Practice-Based Research Network. J Am Dent Assoc. 2014; 145(11):1112–1118. [PubMed: 25359642]
9. Bader JD, Shugars DA. The evidence supporting alternative management strategies for early occlusal caries and suspected occlusal dentinal caries. J Evid Based Dent Pract. 2006; 6(1):91–100. [PubMed: 17138407]
10. Bader JD, Shugars DA, Bonito AJ. A systematic review of the performance of methods for identifying carious lesions. Journal of Public Health Dentistry. 2002; 62(4):201–213. [PubMed: 12474624]
11. Fried D, Featherstone JDB, Glena RE, Seka W. The nature of light scattering in dental enamel and dentin at visible and near-IR wavelengths. Appl Optics. 1995; 34(7):1278–1285.
12. Jones RS, Fried D. Attenuation of 1310-nm and 1550-nm Laser Light through Sound Dental Enamel. Lasers in Dentistry VIII; 2002. Proc SPIE. Vol. 4610. :187–190.
13. Buhler C, Ngaotheppitak P, Fried D. Imaging of occlusal dental caries (decay) with near-IR light at 1310-nm. Optics Express. 2005; 13(2):573–582. [PubMed: 19488387]
14. Fried D, Featherstone JDB, Darling CL, Jones RS, Ngaotheppitak P, Buehler CM. Early Caries Imaging and Monitoring with Near-IR Light. Dental Clinics of North America - Incipient and Hidden Caries. 2005; 49(4):771–794.
15. Hirasuna K, Fried D, Darling CL. Near-IR imaging of developmental defects in dental enamel. J Biomed Opt. 2008; 13(4):044011. [PubMed: 19021339]
16. Staninec M, Lee C, Darling CL, Fried D. In vivo near-IR imaging of approximal dental decay at 1,310 nm. Lasers Surg Med. 2010; 42(4):292–298. [PubMed: 20432277]
17. Lee C, Lee D, Darling CL, Fried D. Nondestructive assessment of the severity of occlusal caries lesions with near-infrared imaging at 1310 nm. J Biomed Opt. 2010; 15(4):047011. [PubMed: 20799842]
18. Darling CL, Huynh GD, Fried D. Light Scattering Properties of Natural and Artificially Demineralized Dental Enamel at 1310-nm. J Biomed Opt. 2006; 11(3):034023.
19. Kuhnisch J, Sochtig F, Pitchika V, Laubender R, Neuhaus KW, Lussi A, Hickel R. In vivo validation of near-infrared light transillumination for interproximal dentin caries detection. Clin Oral Investig. 2015; 20(4):821–829.
20. Sochtig F, Hickel R, Kuhnisch J. Caries detection and diagnostics with near-infrared light transillumination: clinical experiences. Quintessence Int. 2014; 45(6):531–538. [PubMed: 24618570]
21. Jones G, Jones RS, Fried D. Transillumination of interproximal caries lesions with 830-nm light. Lasers in Dentistry X; 2004. SPIE. Vol. 5313. :17–22.
22. Karlsson L, Maia AMA, Kyotoku BBC, Tranaeus S, Gomes ASL, Margulis W. Near-infrared transillumination of teeth: measurement of a system performance. J Biomed Opt. 2010; 15(3): 036001. [PubMed: 20615003]
23. Zakian C, Pretty I, Ellwood R. Near-infrared hyperspectral imaging of teeth for dental caries detection. J Biomed Opt. 2009; 14(6):064047. [PubMed: 20059285]

24. Almaz EC, Simon JC, Fried D, Darling CL. Influence of stains on lesion contrast in the pits and fissures of tooth occlusal surfaces from 800–1600-nm. Lasers in Dentistry XXII; 2016. Proc. of SPIE Vol. 9692. :0U 1–0U 6.
25. Chung S, Fried D, Staninec M, Darling CL. Multispectral near-IR reflectance and transillumination imaging of teeth. Biomed Opt Express. 2011; 2(10):2804–2814. [PubMed: 22025986]
26. Chong SL, Darling CL, Fried D. Nondestructive measurement of the inhibition of demineralization on smooth surfaces using polarization-sensitive optical coherence tomography. Lasers Surg Med. 2007; 39(5):422–427. [PubMed: 17565731]
27. Wu J, Fried D. High contrast near-infrared polarized reflectance images of demineralization on tooth buccal and occlusal surfaces at lambda = 1310-nm. Lasers Surg Med. 2009; 41(3):208–213. [PubMed: 19291753]
28. Fried D, Staninec M, Darling CL, Kang H, Chan K. In vivo Near-IR Imaging of Occlusal Lesions at 1310-nm. Lasers in Dentistry XVII; 2011. Proc. of SPIE. Vol. 7884. :78840:B1–78840:B7.
29. Fried WA, Darling CL, Chan K, Fried D. High Contrast Reflectance Imaging of Simulated Lesions on Tooth Occlusal Surfaces at Near-IR Wavelengths. Lasers Surg Med. 2013; 45(8):533–541. [PubMed: 23857066]
30. Simon JC, Chan KH, Darling CL, Fried D. Multispectral near-IR reflectance imaging of simulated early occlusal lesions: variation of lesion contrast with lesion depth and severity. Lasers Surg Med. 2014; 46(3):203–215. [PubMed: 24375543]
31. Bouma, BE., Tearney, GJ. Handbook of Optical Coherence Tomography. New York, NY: Marcel Dekker; 2002.
32. Colston B, Everett M, Da Silva L, Otis L, Stroeve P, Nathel H. Imaging of hard and soft tissue structure in the oral cavity by optical coherence tomography. Applied Optics. 1998; 37(19):3582–3585. [PubMed: 18273327]
33. Feldchtein FI, Gelikonov GV, Gelikonov VM, Iksanov RR, Kuranov RV, Sergeev AM, Gladkova ND, Ourutina MN, Warren JA, Reitze DH. In vivo OCT imaging of hard and soft tissue of the oral cavity. Optics Express. 1998; 3(3):239–251. [PubMed: 19384366]
34. Baumgartner A, Dicht S, Hitzenberger CK, Sattmann H, Robi B, Moritz A, Sperr W, Fercher AF. Polarization-sensitive optical optical coherence tomography of dental structures. Caries Res. 2000; 34:59–69. [PubMed: 10601786]
35. Fried D, Xie J, Shafi S, Featherstone JD, Breunig TM, Le C. Imaging caries lesions and lesion progression with polarization sensitive optical coherence tomography. J Biomed Opt. 2002; 7(4): 618–627. [PubMed: 12421130]
36. Jones RS, Fried D. The Effect of High Index Liquids on PS-OCT Imaging of Dental Caries. Lasers in Dentistry XI; 2005. SPIE. Vol. 5687. :34–41.
37. Ngaotheppitak P, Darling CL, Fried D. Polarization Optical Coherence Tomography for the Measuring the Severity of Caries Lesions. Lasers Surg Med. 2005; 37(1):78–88. [PubMed: 15889402]
38. Staninec M, Douglas SM, Darling CL, Chan K, Kang H, Lee RC, Fried D. Nondestructive Clinical Assessment of Occlusal Caries Lesions using Near-IR Imaging Methods. Lasers Surg Med. 2011; 43(10):951–959. [PubMed: 22109697]
39. Simon JC, Lucas SA, Lee RC, Staninec M, Tom H, Chan KH, Darling CL, Fried D. Near-IR Transillumination and Reflectance Imaging at 1300-nm and 1500–1700-nm for in vivo Caries Detection. Lasers Surg Med. 2016; 48(9) 828-836-959.
40. Logan CM, Co KU, Fried WA, Simon JC, Staninec M, Fried D, Darling CL. Multispectral near-infrared imaging of composite restorations in extracted teeth. Lasers in Dentistry XX; 2014. Proc. of SPIE Vol. 89290. :1–5.
41. Tom H, Simon JC, Chan KH, Darling CL, Fried D. Near-infrared imaging of demineralization under sealants. J Biomed Opt. 2014; 19(7):77003. [PubMed: 25036214]
42. Simon JC, AL S, Lee RC, Darling CL, Staninec M, Vaderhobli R, Pelzner R, Fried D. Near-infrared imaging of secondary caries lesions around composite restorations at wavelengths from 1300–1700-nm. Dent Mater. 2016; 32(4):587–595. [PubMed: 26876234]

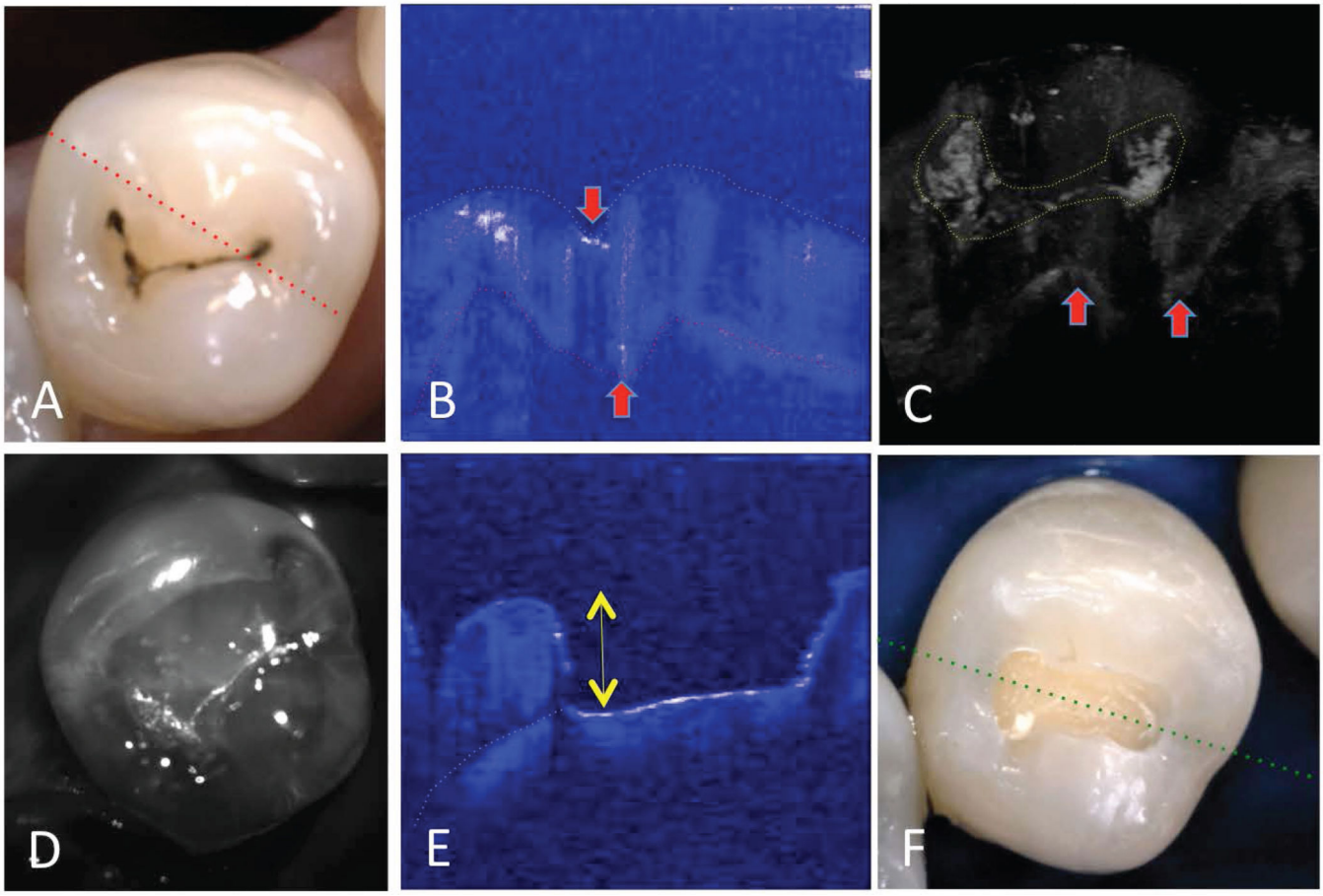

Fig. 1.

Example of an occlusal lesion in which the penetration of the lesion beyond the DEJ is apparent in the CP-OCT image. (A) Visible light reflectance image of the tooth, (B) CP-OCT b-scan image extracted at the position of the red dotted line in (A). The downward pointing red arrow indicates demineralization at the surface of the fissure which blocks penetration of light below it while the upward pointing arrow shows the increased reflectance at the position of the DEJ indicating that the lesion has spread laterally in the dentin. The yellow and red dotted lines indicate the position of the tooth surface and the DEJ. (C) A 3D volumetric rendering of the entire 6 × 6 × 7-mm CP-OCT image shows the lesion at the tooth surface indicated by the high reflectivity in white surrounded by yellow dots. Below the surface between the position of the two red arrows there is a complete loss of reflectivity just below the lesion and increased reflectivity at the DEJ at the position of each red arrow. (D) A near-IR reflectance image of the tooth. (E) CP-OCT b-scan across the cavity preparation at the position of the green dotted line in the visible reflectance image of (F). The cavity depth indicated by the yellow arrow is 2.16-mm. (note attached video file of Fig. 1C - 3D CP-OCT image - movie1.mpg)

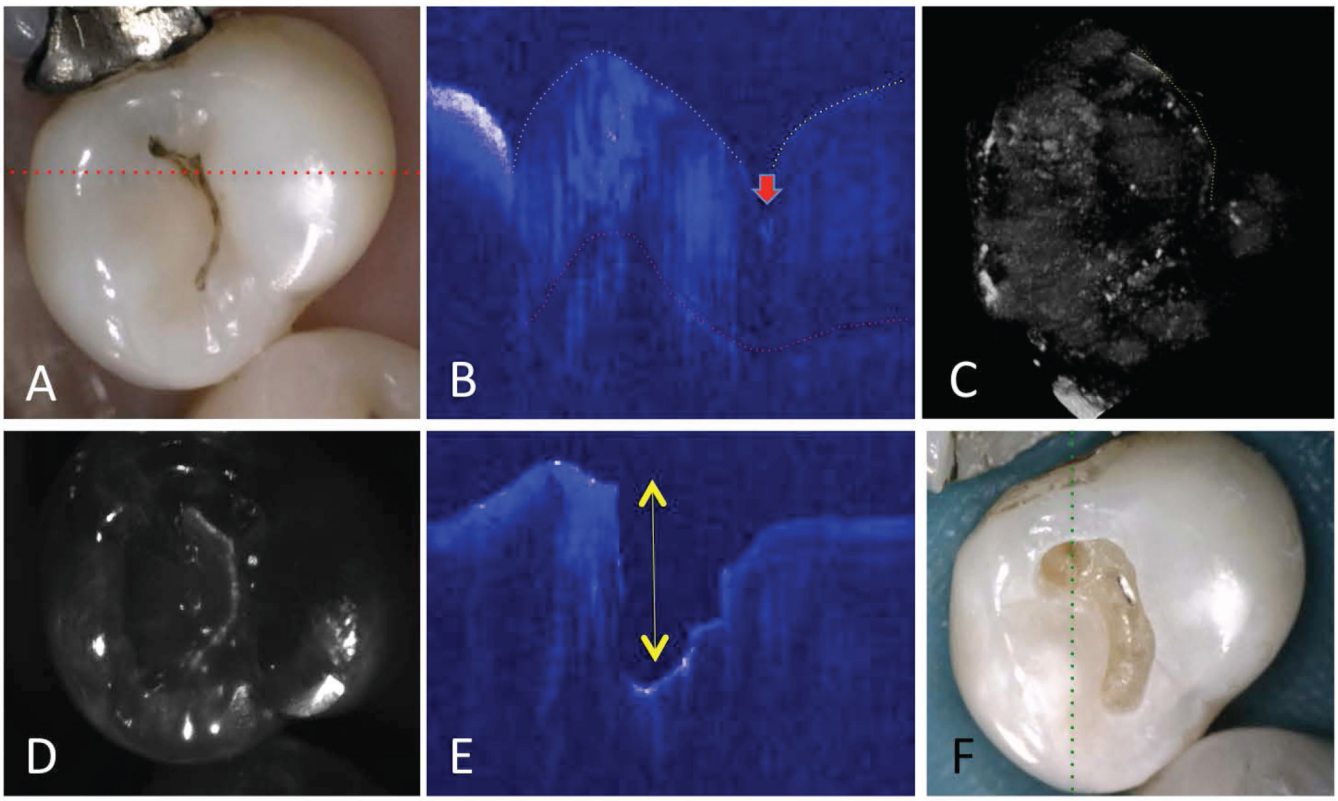

Fig. 2.

Example of an occlusal lesion in which the penetration of the lesion beyond the DEJ was not apparent in the CP-OCT image. (A) Visible light reflectance image of the tooth, (B) CP-OCT b-scan image extracted at the position of the red dotted line in (A). The red arrow indicates the position of the small v-shaped lesion in the fissure. (C) The 3D volumetric rendering of the CP-OCT image shows some increased reflectivity in the fissure at the position indicated by the yellow dotted line. No rise in the subsurface reflectivity is evident. (D) Near-IR reflectance image of the tooth. (E) CP-OCT b-scan across the cavity preparation at the position of the green dotted line in the visible reflectance image of (F). The cavity depth indicated by the yellow arrow is 1.93-mm.

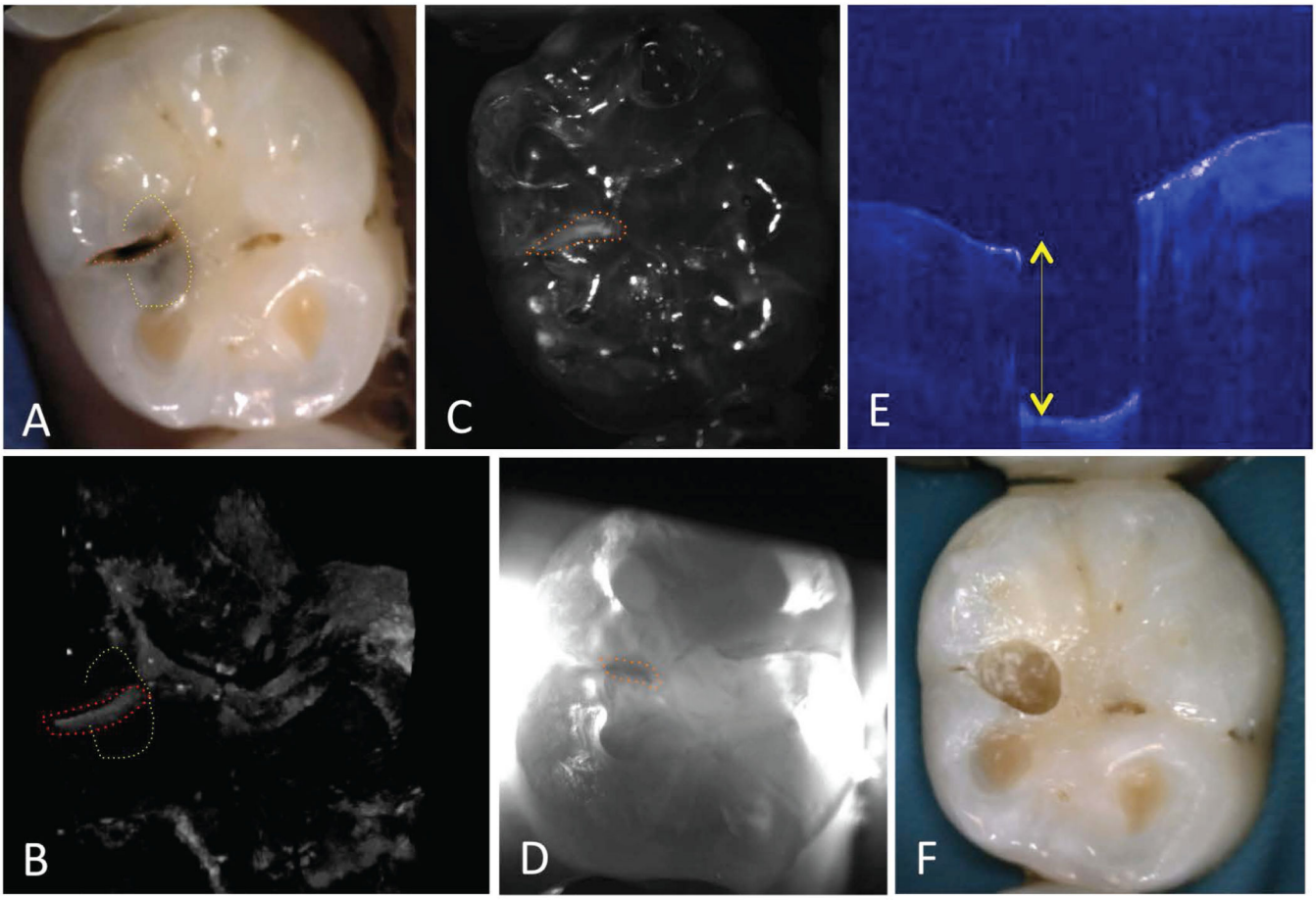

Fig. 3.

An occlusal lesion that manifested a distinct shadow perpheral to the stained fissure. (A) Visible light reflectance image of the tooth, (B) The 3D volumetric rendering of the CP-OCT image shows some increased reflectivity in the fissure at the position surrounded by the red dots. There is no rise in the subsurface reflectivity in the area of the shadow demarcated by the yellow dots. (C) Near-IR reflectance image and (D) near-IR occlusal transillumination image (E) CP-OCT b-scan across the cavity preparation at the position of the green dotted line in the visible reflectance image of (F). The cavity depth indicated by the yellow arrow is 2.59-mm.

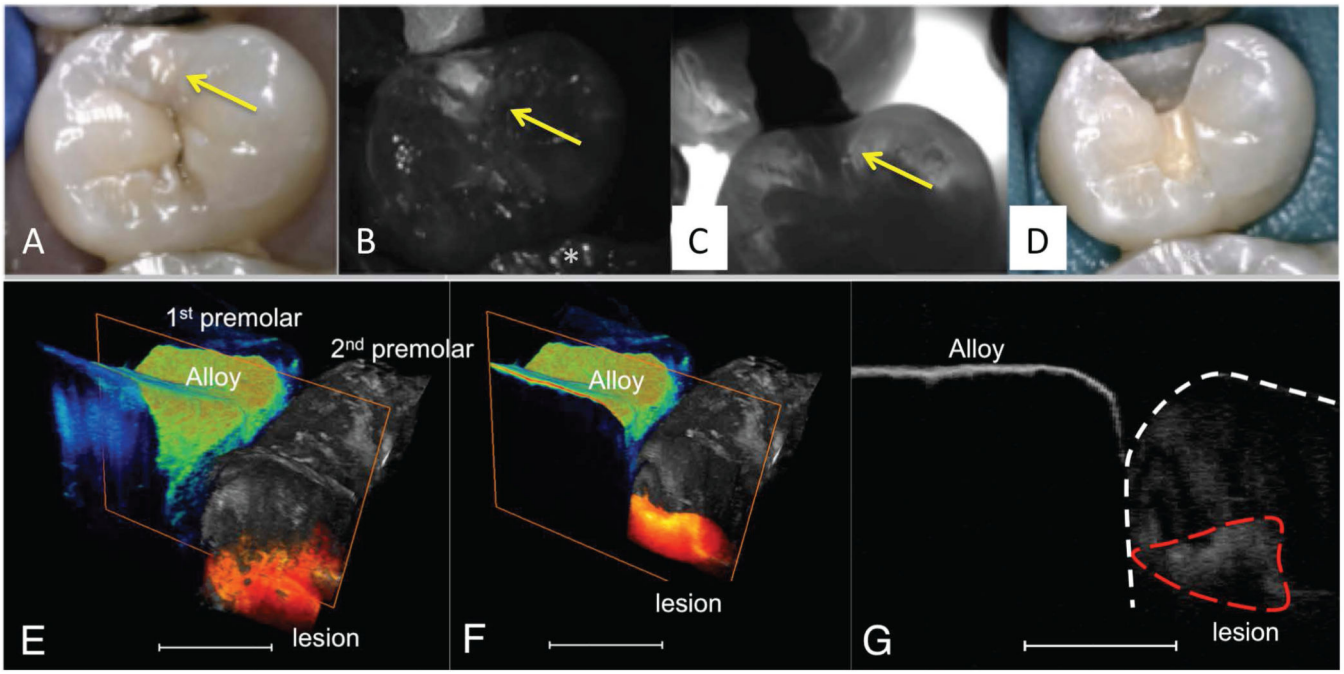

Fig. 4.

Images of a tooth with a suspected occlusal lesion in the central fissure (stained fissure) and an interproximal lesion indicated at the position of the yellow arrow in the visible light reflectance image (A) of the tooth are shown. Near-IR reflectance (B) and near-IR occlusal transillumination images (C) Visible image of the preparation (D) are also shown. A rendered CP-OCT 3D image (E) shows the amalgam (alloy) filling on the adjoining 1st premolar in green and the lesion in red. The length of the bar in images (E-G) is 300-μm. In (F) the same 3D CP-OCT image is shown with the image truncated at the position of the extracted b-scan shown in (F) to better show the lesion. In the extracted b-scan (G) the surface of the 2nd premolar and the subsurface lesion are shown by the white and red dashed lines, respectively.

Table 1

Mean lesion contrast values (SD) and the depth of the cavity preparation (n=25) along with the depth of lesion penetration for the n=13 samples that penetrated beyond the DEJ. I_L is the lesion intensity and I_S is the intensity of the surrounding sound area.

Imaging Method (n=25)	Mean Lesion Contrast (SD)
Reflectance (400–700-nm) **(I_L-I_s)**	−37.9 (14.6)
Reflectance (1500–1700-nm) **(I_L-I_s)**	46.7 (7.1) *
Occlusal Transillumination (1300-nm)	25.9 (7.7)
CP-OCT (Lesion Penetration) n=13	2.4 mm (0.7)
CP-OCT (Preparation Depth) n=25	3.2 mm (0.5)
CP-OCT (Preparation Depth) n=13 (lateral spread evident)	2.5 mm (0.9)
CP-OCT (Preparation Depth) n=12 (no lateral spread evident)	2.3 mm (0.6)

* The lesion contrast was significantly higher for near-IR reflectance at 1500–1700-nm (P<0.05).